THERMAL AGE AND SEAFLOOR TOPOGRAPHY INFERRED FROM A GLOBAL SEISMIC MODEL

M.H. Ritzwoller, N.M. Shapiro, S. Zhong, W. Landuyt, and G.M. Leahy

Center for Imaging the Earth's Interior, University of Colorado at Boulder, Campus Box 390, Boulder, CO, 80309-0390, E-mail: ritzwoll@merckx.colorado.edu

I. Summary

We present a new seismic model of the lithosphere/asthenosphere underlying the Pacific ocean to a depth of about 300 km. The data-set consists of broad-band Rayleigh and Love wave group-velocity (CU-Boulder; 15 - 200 s) and phase-velocity (Harvard, Utrecht; 40 - 150 s) dispersion curves. We construct the group and phase velocity maps using "diffraction tomography" which accounts for path-length dependent sensitivity, wave-form healing and associated diffraction effects that are particularly important for long ocean-crossing paths. Monte-Carlo inversion of the dispersion maps produces an ensemble of acceptable shear velocity models of the crust and uppermost mantle from which average characteristics and uncertainties are extracted. The dispersion velocities and the intrinsic shear velocities of the lithosphere correlate strongly with age, but lithospheric thickening appears to be arrested in two age ranges: 70 - 100 Ma and >130 Ma.

To illuminate these features, we convert the seismic model into temperature and density in order to compare the predicted isotherms and seafloor topography with physical models of lithospheric formation and cooling. We summarize the temperature model by estimating "thermal age", which is the age of the cooling conductive, half-space most similar to the temperature profile at this point. We find:

1. The thermal age of the Pacific lithosphere diverges from the lithospheric age along a strip in the mid-Pacific at ages between 70 - 100 Ma. They diverge again at much older ages > 130 Ma. Divergence of the thermal age from the lithospheric age indicates that the cooling history has deviated from half-space conductive cooling.

2. At ages younger than about 70 Ma, the topography predicted from the seismic model agrees very well with the square-root of age fall-off of conductive cooling except for very young oceanic lithosphere. Between 70 - 100 Ma and again at ages greater than 130 Ma, the inferred topography elevates above the topography expected by conductive cooling alone. In the old Pacific, topography from the seismic model is, on average, elevated above the conductive half-space topography by about 500 m.

These observations provide evidence for the "punctuated cooling of the Pacific lithosphere", in which conductive cooling proceeds in two stages: Stage 1 from 0 to ~70 Ma and, Stage 2 from ~100 to ~130 Ma. The cause of this cooling history remains unclear. The formation of instabilities as the the Pacific lithosphere ages may cause the arrested cooling between 70 - 100 Ma. Stage 2 cooling is a new insight into oceanic mantle dynamics, but its understanding provides a significant theoretical challenge.

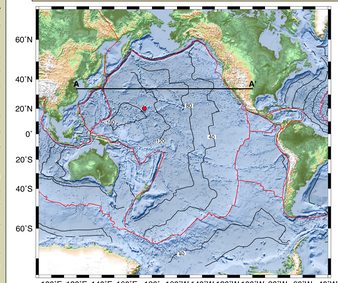

Figure 1. Reference map. The line A - A' corresponds to the vertical slice shown in **Figure 11** and the model beneath the red circle is shown in **Figure 9**. Lithospheric isochrons with a 40 Ma separation are shown as black lines across the Pacific.

II. Data and surface wave tomography

Data Set.
The data are fundamental mode dispersion measurements. Group velocitiesare measured at CU-Boulder using the method described by Ritzwoller and Levshin (1998). The global group velocity data set includes measurements obtained at 561 different stations following 4783 events which generates about 130,000 paths. **Figure 2** shows event and station locations and **Figures 3 and 4** display path coverage. Phase velocity measurements from 40 s - 150 s were obtained at Harvard and Utrecht Universities (Trampert and Woodhouse, 1995; Ekstrom et al., 1997).

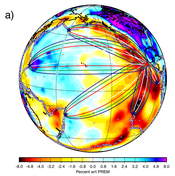

Figure 2. (a) First Fresnel zones plotted over the shear velocity model at 80 km depth for waves observed in Mexico (red triangle) originating from several epicentral regions (red star): Galapagos (2087 km), EPR (4493 km), Aleutians (7777 km), Tonga (8916 km), Marianas (11700). The Fresnel zones are for 20 s (white), 50 s (red), 100 s (green), and 150 s (blue) Rayleigh waves. Stations and events used in the group velocity data set are shown as small red triangles and blue circles, respectively.
(b) The transverse amplitude of the scattering sensitivity kernel at the center of the source-receiver path for 50 s Rayleigh wave phase velocity. The blue and red lines are the Born approximation kernels (Spetzler and Snieder, 2001) for epicentral distances of 2000 km and 8000 km, respectively. The blue and red shaded regions illustrate the crude box-car approximation to the scattering kernels we currently use in "diffraction tomography".

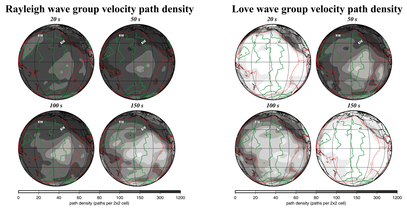

Figures 3 and 4. Group velocity path density across the Pacific. Path density is defined as the number of rays intersecting each 2^0x2^0 grid cell (~50,000 km^2). A path density greater than ~20 rays/cell is needed to construct a minimally reliable tomographic image for the cell.

Diffraction Tomography.
The surface wave dispersion maps result from a surface wave tomographic method that we call "diffraction tomography" which is based on a physical model of the surface wave Fresnel zone rather than on ray-theory and ad-hoc regularization (e.g., Barmin et al., 2001). Diffraction tomography accounts for path-length dependent sensitivity, wave-form healing and associated diffraction effects, and provides a more accurate assessment of spatially variable resolution than traditional tomographic methods. It is inspired by the pioneering efforts of Woodhouse and Girnius (1982), Wielandt (1987), Dahlen et al. (2000), Nolet and Dahlen (2000), Spetzler and Snieder (2001), and others. Recent group and phase velocity maps are shown in **Figures 5 and 6**. Resolution estimates for Rayleigh waves appear in **Figures 7 and 8**.

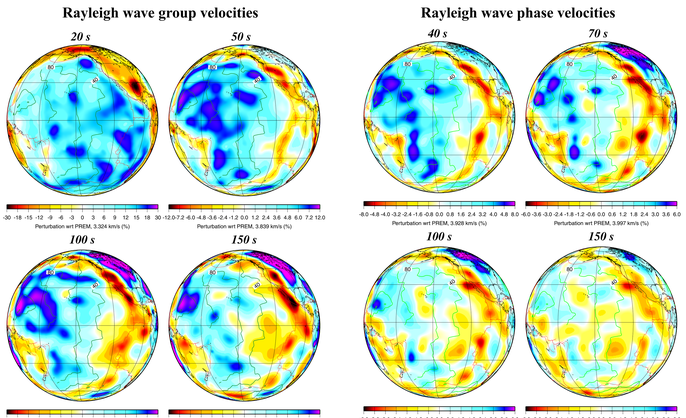

Figures 5 and 6. Sampling of surface wave group and phase velocity maps constructed with "diffraction tomography" which is based on a physical model of surface wave sensitivity within the the first Fresnel zone. Lithospheric ages with a 40 Ma separation are shown as green lines.

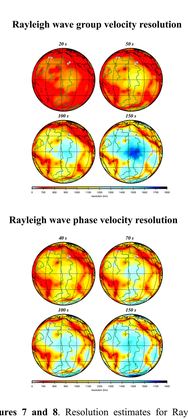

Figures 7 and 8. Resolution estimates for Rayleigh waves based on "diffraction tomography". Resolution is controlled by the average width of the Fresnel zone at each spatial location. Because Fresnel zones are widest in the middle of long paths and taper near source and receiver, resolution degrades toward the mid-Pacific particularly at long periods. Resolution is best in seismogenic regions and near stations.

III. Seismic model

Model Construction.
The shear velocity model is constructed on a 2^0x2^0 grid globally to a depth of about 400 km using the method of Shapiro and Ritzwoller (2001). The goal of the procedure is to estimate the range of models that fit the dispersion maps subject to the uncertainties in the maps together with a priori information. The procedure culminates in a resampling of model space using a Monte Carlo method to produce a radially anisotropic V_S model. The ensemble of acceptable models is summarized with four numbers at each depth: the middle and the half-width of the corridor of acceptable models for both V_{sh} and V_{sv}. The half-width is an uncertainty estimate, designed to encompass both random and systematic errors. The most robust features of the resulting model are those that appear in every member of the ensemble of acceptable model, which we term "persistent". The results for a point in the Pacific are shown in **Figure 9** and several horizontal and vertical slices are shown in **Figures 10 and 11**.

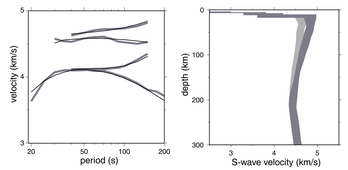

Figure 9. Data and inversion results shown for the point in the central Pacific indicated on **Figure 1**. (LEFT). Observed dispersion curves (thick grey lines, Rayleigh and Love wave group and phase velocity) and fit provided by the shear velocity model (black lines). (RIGHT). The corridors indicate the ensemble of acceptable shear velocity models at each depth. The model is radially anisotropy between Moho and a depth of about 200 km: V_{sh} ne V_{sh}.

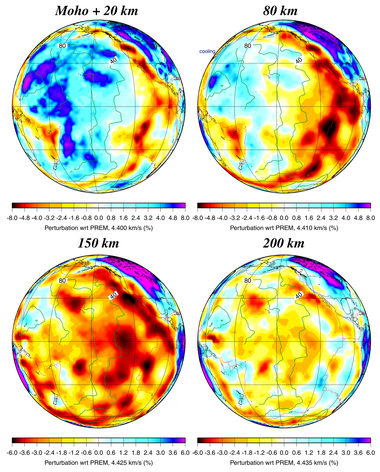

Figure 10. Horizontal slices of the shear velocity model at four depths. Lithospheric ages with a 40 Ma separation are shown as green lines.

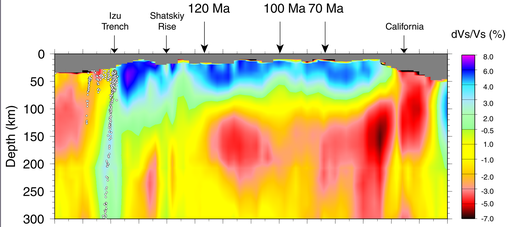

Figure 11. Vertical slice along profile A - A' indicated in **Figure 1**. Note the general thickening of the lithosphere toward the west and the slab subduction at the Izu Trench. Seismic velocities in the lithosphere reduce at ages between 70 - 100 Ma and again between about 120 - 140 Ma.

IV. Seismic velocities versus lithospheric age

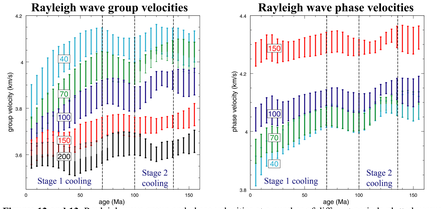

Figures 12 and 13. Rayleigh wave group and phase velocities at a number of different periods plotted versus lithospheric age. The "error bars" indicate the standard deviation of the velocities within a 10 Ma age range. Note that at intermediate periods (40 s - 100 s), which are predominantly sensitive to the oceanic uppermost mantle, velocities increase with age until about 60 Ma and then dip or flatten until about 100 Ma. This signature also can be seen in the original dispersion maps shown in **Figures 5 and 6**.

Surface wave dispersion speeds as a function of period and shear wave velocities as a function of depth strongly depend on lithospheric age across the Pacific. We use the lithospheric age model of Müller et al. (1997) to aggregate surface wave velocities (**Figures 12 and 13**) and 3D model velocities (**Figure 14**) into overlapping 10 Ma age ranges and then compute the average and standard deviation in each range. The surface wave velocities and the shear velocities display systematic trends with lithospheric age. Note that the velocity versus age relations flatten between 70 - 100 Ma and again at ages greater than about 130 Ma.

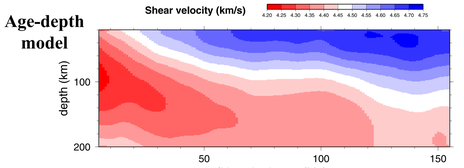

Figure 14. Average shear velocity as a function of lithospheric age and depth. The high velocity lid (lithosphere) thickens with age until about 70 Ma where it flattens until about 100 Ma. It thickens again until about 140 Ma.

V. Converting Vs to temperature and density

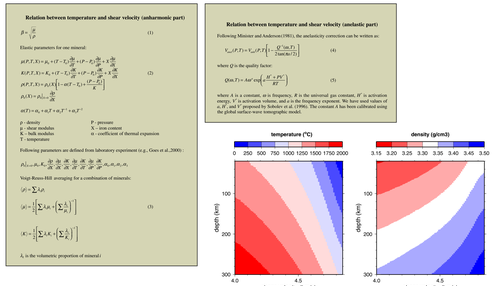

Figure 15. Converting Vs to temperature and density

We use the relations $T(V_S,P)$ and $\rho(V_S,P)$ shown in Figure 15 (Goes et al., 2000) to transform shear velocities to temperature and density as a function of depth. **Figure 16** shows the temperatures estimated from the age-depth model presented in **Figure 14**. The inferred isotherms systematically differ from the isotherms of a conductive half-space: in particular, they flatten between 70 - 100 Ma and again at ages greater than about 130 Ma.

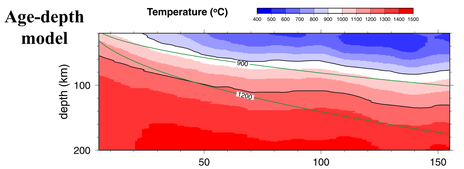

Figure 16. Temperature inferred from the seismic age-depth model shown in **Figure 14**, plotted as a function of depth and lithospheric age. The 900 C and 1200 isotherms are plotted (black contours) and compared with the isotherms from a conductive half-space (green contours).

VI. Thermal age

At each spatial point, the temperature profile inferred from the seismic shear velocities can be summized by the "thermal age"; that is, the age of the cooling conductive, half-space most similar to the temperature profile at this point. An example is shown in **Figure 17**, displayed across the entire Pacific in **Figure 18**, and aggregated by lithospheric age in **Figure 19**. Divergence of the thermal age from the lithospheric age indicates that the cooling history has deviated from simple conductive cooling. We take this as evidence for the effect of convection.

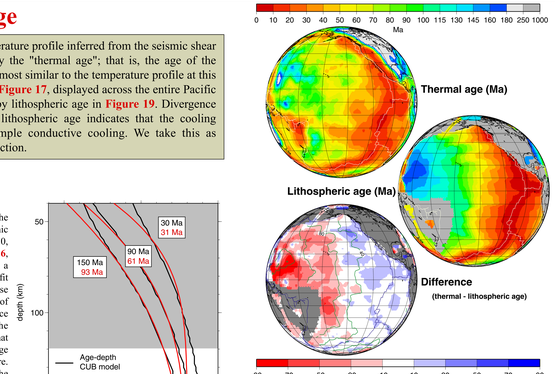

Figure 17. Comparison between the temperatures inferred from the seismic model at three lithospheric ages (30, 90, 150 Ma), taken from **Figure 16**, and the temperature profiles from a condutive, cooling half-space that fit these profiles best in a 1-norm sense between 40 - 120 km depth. The age of the best-fitting conductive half-space temperature profile defines the "thermal age" of the model. Note that the lithospheric age and thermal age are similar for the 30 Ma lithosphere. The thermal age is lower than the lithospheric age for Pacific lithosphere older than about 70 Ma.

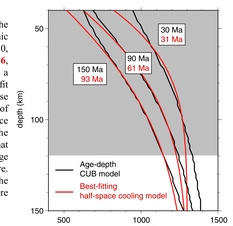

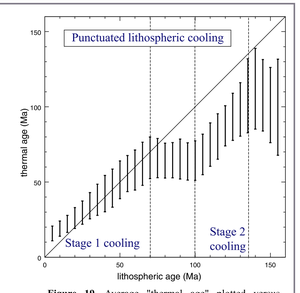

Figure 18. Summary comparison of "thermal age" and lithospheric age (Mueller et al., 1997). The thermal age of the Pacific lithosphere begins to diverge from the lithospheric age along a stripe of about 70 Ma in the mid-Pacific. They diverge further at much older ages.

Figure 19. Average "thermal age" plotted versus lithospheric age for the Pacific. Error bars indicate the standard deviation of thermal age in 10 Ma lithospheric age ranges. Results summarize **Figure 18**. Trends at 45 degrees indicate cooling similar to conductive, half-space cooling. A flatter slope indicates arrested cooling. Lithospheric cooling appears to be arrested between 70 - 100 Ma and again at ages greater than 130 Ma. This demonstrates the "punctuated cooling" of the Pacific lithosphere.

VII. Seafloor topography

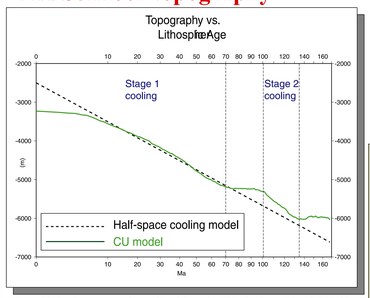

Figure 20. Seafloor topography predicted from the CU seismic model and the half-space cooling model

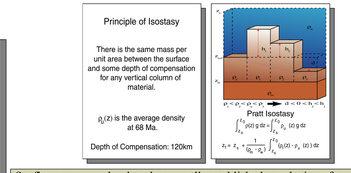

Seafloor topography has been well established to deviate from topography predicted from a cooling conductive, half-space (e.g., Stein and Stein, 1992). Conversion of the seismic shear velocity model into density (**Figure 15**), allows seafloor topography to be estimated by applying Pratt isostasy. **Figure 20** compares half-space cooling topography with topography predicted from the seismic model in this way. At ages younger than about 70 Ma, the topography predicted from the seismic model agrees very well with thesquare-root of age fall-off of conductive cooling except for very young oceanic lithosphere. Between 70 - 100 Ma and again at ages greater than 130 Ma, the inferred topography elevates above the topography expected by half-space conductive cooling alone. In the old Pacific, topography from the seismic model is, on average, elevated above the conductive topography by about 500 m.

Acknowledgment
We gratefully acknowledge the phase velocities measurements that were obtained by researchers at Harvard University and Utrecht University.

References

Barmin, M.P., M.H. Ritzwoller, and A.L. Levshin, A fast and reliable method for surface wave tomography, *Pure appl. geophys.*, **158**, 1351-1375, 2001.

Dahlen, F.A., S.H. Hung, and G. Nolet, Frechet kernels for finite-frequency travel times: I. Theory, *Geophys. J. Int.*, **141**, 157-174, 2000.

Ekstrom, G., J. Tromp, and E.W.F. Larson, Measurements and global models of surface wave propagation, *J. Geophys. Res.*, **102**, 8137-8158, 1997.

Goes, S., R. Govers, and P. Vacher, Shallow mantle temperatures under Europe from P and S wave tomography, *J. Geophys. Res.*, **105**, 11,153-11,169, 2000.

Müller, R.D., Roest, W.R., Royer, J.-Y., Gahagan, L.M., and Sclater, J.G., Digital isochrons of the world's ocean floor, *J. Geophys. Res.*, **102**, 3211-3214, 1997.

Nolet, G. and F.A. Dahlen, Wave front healing and the evolution of seismic delay times, *J. Geophys. Res.*, **105**, 19,043-19,054, 2000.

Shapiro, N.M. and M.H. Ritzwoller, Monte Carlo inversion of broad band surface wave dispersion for a global shear velocity model of the crust and upper mantle, *Geophys. J. Int.*, submitted, 2001.

Spetzler, J. and R. Snieder, Are we exceeding the limits of the great circle approximation in global surface wave tomography? *Geophys. Res. Lett.*, **28**, 2341-2344, 2001.

Stein, C.A. and S. Stein, A model for the global variation in oceanic depth and heat flow with lithospheric age, *Nature*, **359**, 123-129, 1992.

Trampert, J., and J. Woodhouse, Global phase velocity maps of Love and Rayleigh waves between 40 and 150 seconds, *Geophys. J. Int.*, **122**, 675 - 690, 1995.

Woodhouse, J.H. and T.P. Girnius, Surface waves and free oscillations in a regionalized earth model, *Geophys. J. R. Astr. Soc.*, **68**, 653-673, 1982.